HOSTED BY
ELSEVIER
CrossMark
Available online at www.sciencedirect.com
ScienceDirect
Defence Technology 12 (2016) 159–170
www.elsevier.com/locate/dt

On the study of ricochet and penetration in sand, water and gelatin by spheres, 7.62 mm APM2, and 25 mm projectiles

John F. MOXNES [a,*], Øyvind FRØYLAND [a], Stian SKRIUDALEN [a], Anne K. PRYTZ [b], Jan A. TELAND [a], Eva FRIIS [b], Gard ØDEGÅRDSTUEN [b]

[a] *Land Systems Division, Norwegian Defence Research Establishment, P.O. Box 25, NO-2027 Kjeller, Norway*
[b] *Nammo Raufoss AS, P.O. Box 162, NO-2831 Raufoss, Norway*

Received 4 August 2015; revised 16 December 2015; accepted 17 December 2015
Available online 8 January 2016

Abstract

We examine the ricochet and penetration behavior in sand, water and gelatin by steel spheres, 7.62 mm APM2 and 25 mm projectiles. A threshold impact angle (critical angle) exists beyond which ricochet cannot occur. The Autodyn simulation code with the smooth particle hydrodynamic (SPH) method and Impetus Afea Solver with the corpuscular model are used and the results are compared with experimental and analytical results. The resistance force in sand for spheres was proportional to a term quadratic in velocity plus a term linear in velocity. The drag coefficient for the quadratic term was 0.65. The Autodyn and Impetus Afea codes simulate too large penetration due to the lack of a linear velocity resistance force. Critical ricochet angles were consistent with analytical results in the literature. In ballistic gelatin at velocities of 50–850 m/s a drag coefficient of 0.30 fits the high speed camera recordings if a linear velocity resistance term is included. However, only a quadratic velocity resistance force with drag coefficient that varies with the Reynolds number also fits the measurements. The simulation of a sphere in water with Autodyn showed too large drag coefficient. The 7.62 mm APM2 core simulations in sand fit reasonable well for both codes. The 25 mm projectile ricochet simulations in sand show consistency with the high speed camera recordings. Computer time was reduced by one to two orders of magnitudes when applying the Impetus Afea Solver compared to Autodyn code due to the use of the graphics processing units (GPU).

Keywords: Ricochet; Simulation; Sand; Gelatin; Autodyn; Impetus Afea Solver; Smooth particle; Sphere

1. Introduction

Ricochet occurs when the final velocity vector of the center of mass of a projectile is oriented away from the target and is associated with small impact angles or high obliquity (obliquity is defined as the angle between the normal surface vector and the velocity vector of the center of mass of the projectile). The ricochet angle and the ricochet velocity are dependent on the impact velocity, obliquity angle, yaw, mass of the projectile, geometry, moment of inertia and target properties. A threshold impact angle (critical angle) exists beyond which ricochet cannot occur. However, the relationship between critical impact angle, projectile nose shape, amount of water, mineralogy and impact velocity is still not fully understood [1].

1.1. Sand

Sand grain failure in front of the projectile may be an important energy dissipation mechanism in sand. Very fine white powder is observed in the wake of the projectile due to the pulverization in front of the projectile. It has been estimated that 8% of the energy of the projectile was consumed in pulverization of the individual sand particles in hypersonic sand penetration experiments [2]. The yield point during compressing of aggregate sand can be correlated to the initiation of particle failure [3]. When sand is under loading it undergoes a change in shape and compressibility. The volume decreases due to changes in grain arrangements where microscopic interlocking with frictional forces between interacting particles lead to bending of flat grains and rolling of rounded particles. If the load is further increased, the grains eventually become crushed. High pressure compression tests have revealed different types of damage mechanisms, (a) single abrasion fracture, (b) multiple abrasion fractures, (c) major splitting of particles into two or more particles, (d) breakage of sub particles,

Peer review under responsibility of China Ordnance Society.
* Corresponding author. Tel.: +47 63 807514.
E-mail address: john-f.moxnes@ffi.no (J.F. MOXNES).

http://dx.doi.org/10.1016/j.dt.2015.12.004
2214-9147/

(e) pulverization of particles into many small pieces. However, under high rate compressive loading, the only mode of failure observed was pulverization, Parab et al. [4]. At very low velocities frictional resistance exceeds hydrodynamic resistance. At projectile velocities above the speed of sound in the sand, particles may lock up instead of flowing locally. However, lock up of particles may depend on the density. The difference in response for high and low velocity is related to the timescale required for relaxation of force chain structures. A comprehensive review of the response of granular media to rapid penetration was recently published by Omidvar et al. [5].

1.2. Modeling

Modeling by discrete element methods may require extensive material parameters at high strain rates, large strain, and high pressure. Use of simple analytical models is thus for some cases a viable alternative. When the deformation of the projectile is negligible the rigid body assumption can be applied. For linear projectile trajectories Robins [6] and Euler [7] assumed that for sand the force was a constant. Poncelet [8] set the force equal to a constant plus a term proportional to the square of the velocity. Resal [9] set the force proportional to the velocity plus a term proportional to the square of the velocity. Forrestal and Luk [10] applied a force that was a constant plus a term proportional to the square of the velocity based on the cavity expansion theory. Agreement within 19% was shown when comparing with experimental results. Allen et al. [11] developed a model where an abrupt transition in drag force occurs at the critical velocity, of about 100 m/s, believed to be due to transition from inelastic to quasi-elastic impacts. Projectiles with nose cone angles from 180 to 90° were stable. For penetration problems with relative large obliquity, yaw or pitch, nonlinear motion is expected and the projectile may even reverse its motion toward the target surface (ricochet). However, even for very small yaw, or obliquity, instability may occur and the trajectory becomes curved. Soliman et al. [12] studied many years ago spherical projectile ricochet in water and sand theoretically and experimentally. For water and sand it was found that the ricochet angle was around 20% larger than the impact angle. Bernard et al. [13] show that the trajectory went from linear to curved when the impact velocity was increased from 427 to 512 m/s for 3.7° obliquity. Above 30° obliquity the trajectory was curved and the projectile might move towards the target surface when the projectile's slenderness ratio L/D (length to the diameter of the projectile) was reduced. Projectiles with nose cone angles less than 90° become progressively more unstable with decreasing cone angle. For sand it was found that the critical angle decreases with increasing velocity but a cut-off angle was found.

Daneshi and Johnson [14,15], studied ricochet of spherical and dumb-bell shaped projectiles in sand and found that the volume of sand displaced from the crater was proportional to the initial momentum of the projectile. Bai and Johnson [16] examined the effect of projectile speed and medium resistance on ricochet in sand. Johnson et al. [17] examined the effect of high velocity oblique impact and ricochet of mainly long rod projectiles. Savvatteev et al. [18] examined high-speed (up to 4000 m/s) penetration into sand. Full melting of the steel bullets occurs at the velocity of 1800–2000 m/s. Anderson et al. [19] studied the flow field center migration during vertical and oblique impacts. Reducing the friction between grains and projectile increases stability [20]. Bless et al. [21] found that a hemi spherical nose gave less resistance and that projectiles were stabilized by fins. Nishida et al. [22] examined the effect of sand density and projectile diameter on critical incident angles of projectiles impacting granular media. The critical reverse velocity is the velocity where the projectile starts to move back to the surface of the target. Li and Flores-Johnson [23] investigated the trajectory in soil penetration by implementing a resistance function based on the cavity expansion theory into ABAQUS code. It was found that the critical reverse velocity decreases with increasing obliquity and that tumbling of the projectile increases with the ratio L_c/L, where L_c is the distance from the nose of the projectile to the center of mass and L is the length. Ye et al. [24] studied the influence of projectile rotation on the oblique penetration in granular media. See Johnson et al. [17] for a review of high velocity oblique and impact ricochet.

Impacts on gelatin show significantly different displacement fields compared to sand [25]. See also Wen et al. [26] for impact of steel spheres in gelatin at moderate velocities.

Rigorous hydrocode calculations can offer insight into the physics of ricochet. Numerical models have increasingly been used in analysis of projectile penetration into soils and granular materials due to the inherent complexity of the problem. Soil or sand can be considered as a three phase medium consisting mainly of solid grains, with portions of water and air. Moxnes et al. [27] proposed a continuum MO-granular model where parameters are constructed by using a quasi-static unilateral compression test, and validated by using a high-speed piston (up to 300 m/s) impacting a granular pyrotechnic bed. The piston and the tube were made of lexan, which made it possible to record the piston position and the compaction wave propagating in front, by using a high-speed camera. The experimental recordings were compared to numerical simulations, using the explicit numerical code Autodyn-2D, and a new constitutive material model for the porous material. The models apply a hydrostatic compaction curve as a function of the density, a model for the yield stress as a function of pressure and elastic modulus as a function of density. The model does not include any strain rate dependency of yield stress. This is an assumption that may be good as long as the strain rate is above 10^3/s [28]. For a review of stress–strain behavior of sand at high strain rates, see Omidvar et al. [29]. Laine and Sandvik [30] derived quasi static tri-axial material parameters for dry sand using the MO-granular continuum model implemented in Autodyn. The model applies when soil packing density is sufficient high and hence the particle–particle contacts are semi-permanent. We agree with Grujicic et al. [31] that this is the widely used soil model in military communities and it has been widely used for shock simulation involving dry sand within the Autodyn community with quite decent results, e.g. for determining blast load from buried mines [32,33]. However, the model also has been used in civil applications such as road side safety [34]. The

model provides a good compromise between the inclusion of essential physical phenomena reflecting material response under dynamic loading and computational simplicity [31].

The elastic unloading wave in sand travels faster than the plastic compaction wave, which leads to fast attenuation and energy absorption of the propagating wave. Recently Laine and Larsen [35] presented a model where the elastic bulk modulus is both a function of the density and pressure. This modification captures more properly the non-linear behavior seen in tri-axial test data during unloading. The modification results in a more accurate shock wave propagation and attenuation in dry sand. The parameters of Laine and Sandvik [30] were developed essentially for dry sand, and it has to be modified by moisture content. The dry sand material parameters underpredict the magnitude of transferred impulse at high levels of moisture (roughly above 10%) due to too high compressibility of sand that promotes energy dissipating through irreversible compaction of the sand, and lack of consideration of the reduction of the yield stress due to moisture induced inter-particle lubrication effects. Recently Grujicic et al. [31,36] developed a modified version of the Moxnes et al. [27] model with the Laine and Sandvik [30] parameters to account for moisture content. The essential changes are that the compaction curve, yield stress and the elastic modulus are parameterized by the degree of water saturation. A somewhat improved agreement with the experimental results was obtained. For three phase models, see Wang et al. [37], Grujicic et al. [31,36], and Zakrisson et al. [38]. Tong and Tuan [39] used a visco-plastic model with the Drucker–Prager yield criterion for the solid phase along with the capacity of incorporating damage. Higgins et al. [40] developed a model for high strain rate based on the concepts of critical-state soil mechanics.

Although, it is most common to model heterogeneous materials such as sand or powder as a continuum, in so doing the heterogeneous nature of the material and grain interaction are lost. With the continued development of massive computer architectures and parallel processing techniques, sufficiently large domains and high resolution simulations of these heterogeneous materials are feasible such that each grain is assigned material properties. See Andò et al. [41] for recent attempts to track discrete particles and [20,42,43] for a study on two and three dimensional meso-scale simulations.

Deshpande et al. [44] developed a constitutive model, based on the approach proposed by Bagnold [45], for high-rate deformation of an aggregate of monosized rigid spherical particles (corpuscles) that collide and interact by damping and friction. Those particles are not necessarily of the same size as the sand particles. This discrete theory focus on the response of a loose aggregate, particular relevant to ejecta from shallow-buried explosives and the loading structures by high velocity spray of low density soil. The corpuscular approach for sand was further developed by Børvik et al. [46] by combining with an earlier developed corpuscular approach for gases [47,48]. Anderson et al. [49] provided a comprehensive review of the literature related to mine blast and also performed a series of mine blast loading experiments that provide data for numerical simulations and validations of constitutive models. Johnson et al. [50] presented a hybrid particle-finite element algorithm for high velocity impact. Børvik et al. [51] examined the penetration of granular materials by small-arms bullets. The corpuscular approach was used for the sand. A random disturbance was introduced due to the numerical particle stacking. Good agreement with experimental results was achieved.

In section 2 we study experimental and simulation results in sand, gelatin, and water; both during penetration and ricochet. Section 3 concludes.

2. Penetration and ricochet in sand by spheres and 7.62 APM2 projectiles

2.1. Sand

Fig. 1 shows the particle distribution of two different sand types. The Nammo and Børvik et al. [51] sand have much the same distribution. The sand used by Laine and Sandvik [30] is similar we believe. In the Autodyn simulation we use the MO-granular model with the Laine and Sandvik [30] parameters. In Impetus Afea Solver we use the parameters of Børvik et al. [51] and the corpuscular theory. The sand bed sizes are identical in Autodyn and Impetus Afea Solver simulations.

2.2. Numerically

The projectiles are assumed to be rigid, while the target is modeled using smooth particle hydrodynamics (SPH) in Autodyn. In Impetus Afea Solver we, in addition to the rigid model, also use an elastic model of the projectiles. The target is modeled by the corpuscular theory. All simulations in Impetus Afea Solver are run in full 3D, while in Autodyn 3D with half symmetry is chosen.

2.3. Sphere

A steel sphere of radius $a = 0.6$ cm is shot into sand at the impact velocity of 850 m/s and zero obliquity. The density of the sand is 1.82 g/cm^3. The simulations use a bed size of 25 cm × 4.8 cm × 4.8 cm. Particle size is 0.1 cm. The maximum penetration distance was recorded to be 18 cm [18]. Fig. 2 shows the simulated position vs time. Both the Autodyn and the Impetus Afea Solver simulate a somewhat too large penetration position, and the velocity is not zero at the

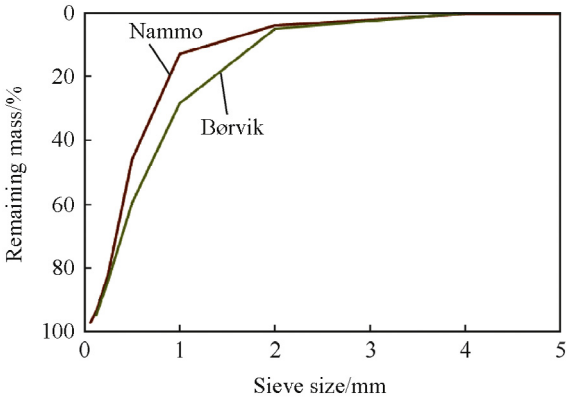

Fig. 1. The remaining mass fraction of the sand as a function of the sieve size.

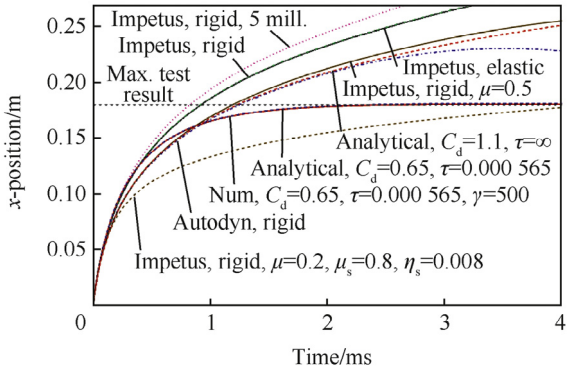

Fig. 2. The position x vs time for a steel sphere with radius $a = 0.6$ cm penetrating sand. The impact velocity is 850 m/s. Horizontal dashed line is measurement of the maximum penetration distance of 18 cm.

penetration distance of 18 cm. We apply an analytical model which gives that the sphere stops at some distance. The resistance force is assumed to be proportional to a sum of a quadratic and linear term in the velocity [9], to read

$$\frac{dv}{dt} = -\frac{v}{\tau} - \frac{1}{2m}\rho C_d A v^2 = -\frac{v}{\tau} - \frac{v^2}{v_c \tau}$$
$$v_c \tau = \frac{1}{\frac{1}{2m}\rho C_d A}, \quad A = \pi a^2 \tag{1}$$

ρ is the density of sand, a is the radius of the sphere, and C_d is the drag coefficient. v_c is a parameter with the unit of velocity while τ is a parameter with dimension time. A is the projected area of the sphere. The solution of Eq. (1) can be written [52]

$$v(t) = \frac{v_0 v_c}{(v_0 + v_c) Exp(t/\tau) - v_0}$$
$$x(t) = v_c \tau \mathrm{Ln}\left(1 + \frac{v_0}{v_c}(1 - \mathrm{Exp}(-t/\tau))\right) \tag{2}$$
$$v(x) = (v_0 + v_c) Exp(-x/(v_c \tau)) - v_c$$

It is easily verified that the maximum penetration length L is

$$v(x) = 0 \Rightarrow L = v_c \tau \mathrm{Ln}\left(1 + \frac{v_0}{v_c}\right) \tag{3}$$

Without the linear resistance term an infinite maximum penetration length is achieved. Interestingly, this solution without the linear velocity resistance term fits to the Autodyn solution for all times when $C_d = 1.1$. We fit the solution in Eq. (2) to τ and C_d (or v_c) such that the maximum penetration length is 18 cm and thus in agreement with the experiments (Fig. 2). But no unique solution exists for the two parameters. However, Savvatteev et al. [18] also applied impact velocities of 1300 m/s and 1580 m/s without significant deformation or melting of the sphere. The maximum penetration length was 22 cm and 24 cm respectively. Using these results we find that $\tau = 5.65 \times 10^{-4}$ s and $C_d = 0.65$ fits well to the three shooting velocities. However, a problem with the solution is that only at infinite time does the solution reach the maximum penetration length. By adding a small resistance term of $\gamma = -500\ \mathrm{m/s^2}$ on the right hand side of Eq. (1) [11], the solution is approximately the same but reaches the final penetration length in finite time.

Impetus Afea Solver results in penetrations larger than in Autodyn (Fig. 2). Applying elastic or a rigid model for the sphere does not influence the results significantly. When increasing particle number from 1 million (baseline) to 5 million the simulated position increases. The position is significantly reduced when applying friction (μ) between the sphere and the sand, and fits the Autodyn result without friction. In a newly developed sand model a cap is introduced in the Impetus Afea Solver (Appendix B). Here the friction force between the sand particles saturates at high contact forces. We apply the baseline parameters $\mu_s = 0.8, \eta_s = 0.008$, and $\mu = 0.2$ (Fig. 2).

We define the effective drag coefficient by

$$C_d^* = -\frac{m\frac{dv}{dt}}{\frac{1}{2}\rho A v^2} \tag{4}$$

Using Eq. (1) the effective drag coefficient is easily shown to be $C_d^* = C_d(1 + 2m/(\rho C_d A \tau v))$. Thus the effective drag coefficient is increasing with decreasing velocity. Fig. 3 shows the different drag coefficients. Autodyn has larger drag coefficient than Impetus Afea Solver and the drag is almost equal to the drag coefficient in Impetus Afea Solver applying a friction coefficient of 0.5 between the sphere and the sand. The analytical model in Eq. (2) shows that the effective drag coefficient increases with decreasing velocity. However, since the velocity of the sphere decreases very fast, the drag coefficient at larger times does not influence the velocity very much (Fig. 4).

Fig. 5 shows the simulations in Autodyn for the steel sphere. It is notable that to simulate the drag the width of the sand bed does not need to be very much larger than the sphere. However, to simulate the correct sand cavity (which is not an issue here) the width of the bed has to be much larger. Larger bed increases the computer time.

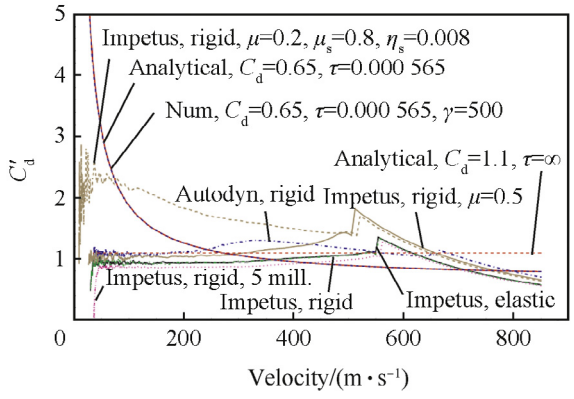

Fig. 3. The different drag coefficients as a function of velocity simulated by Autodyn and Impetus Afea Solver.

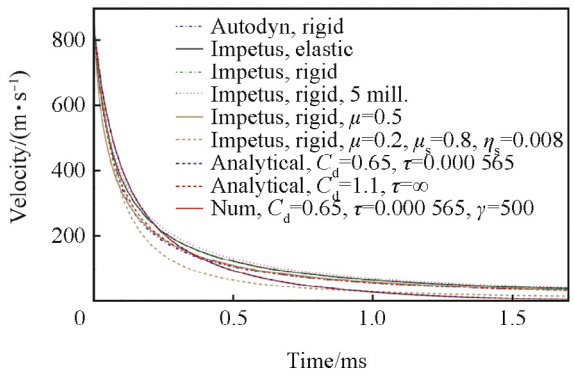

Fig. 4. The velocity vs time for a steel sphere with radius $a = 0.6$ cm penetrating sand. The impact velocity is 850 m/s.

By applying pressure in front of the sphere of $p = 1/2\rho v^2 + K$, it can be shown that the critical ricochet angle is [16]

$$\theta_c = \sqrt{\frac{\rho}{\rho_s}\left(\frac{1}{10} + \frac{K}{\rho v^2}\right) - \frac{4ag}{v^2}} \tag{5}$$

where $\rho_s =$ is the density of the sphere. It is easily verified that the term with the acceleration of gravity g is negligible. We set K equal to the flow stress in sand that depends on the hydrodynamic pressure $1/2\rho v^2$. For the velocity of 850 m/s the hydrodynamic pressure is 3.6×10^8 Pa. Thus the flow stress K is 226 MPa (Appendix A). Inserting into Eq. (5) gives the critical angle of 14° for the steel sphere of density $\rho = 7.8\ \mathrm{g/cm^3}$. For water $K = 0$, $\rho = 1.0\ \mathrm{g/cm^3}$, and we achieve 6° critical angle. Figs. 6 and 7 show the result for two different impact angles. The results are consistent with the analytical model in Eq. (5).

As a further test on the numerical simulations and the analytical model we numerically shot the sphere into water. The results are consistent with the analytical theory as seen in Figs. 8 and 9. However, a closer examination of the drag coefficient, addressed later in this article, shows that Autodyn simulates too large drag coefficient.

We shot a steel sphere of radius $a = 0.25$ cm into ballistic gelatin that had the mass fraction of 90% water and 10% gelatin. The density was 1.02 g/cm^3. The simulation bed is cylindrical with diameter 2.5 cm and length 20 cm. The SPH particle size in the bed is 0.5 mm.

Gelatin has been modeled as an elastic plastic material with yield strength of Y [Pa] $= 2.2 \times 10^5 + 1.9 \times 10^4\ \varepsilon_p$ where ε_p is the effective plastic strain [26]. However, the strength is small compared to the overall hydrodynamic pressure and we neglect it together with any strain rate dependency.

Fig. 10 shows the position vs time for three different impact velocities. A resistance force quadratic in velocity with constant drag coefficient does not fit to the experiments (results not shown). However, if we use the linear term resistance velocity

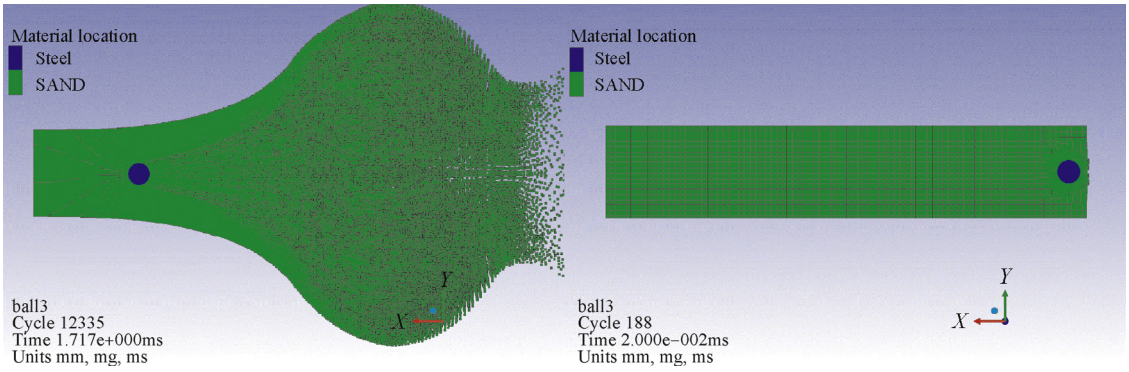

Fig. 5. Penetration of a steel sphere of radius $a = 0.6$ cm in sand. Impact velocity is 850 m/s (Autodyn).

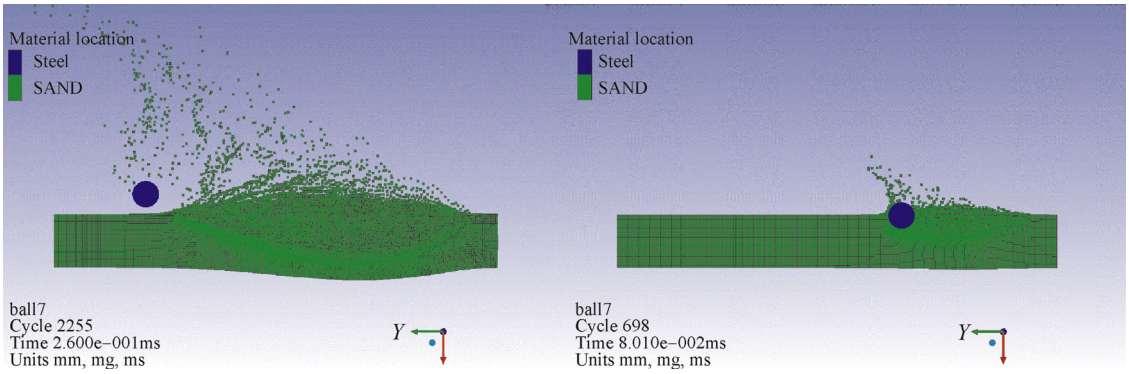

Fig. 6. Ricochet of a steel sphere of radius $a = 0.6$ cm in sand. Impact velocity is 850 m/s and impact angle is 10° (Autodyn).

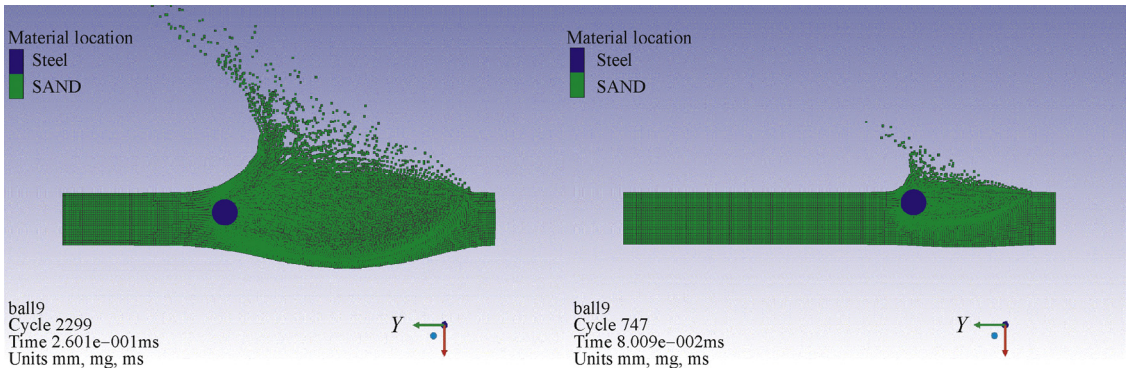

Fig. 7. Penetration of a steel sphere of radius $a = 0.6$ cm in sand. Impact velocity is 850 m/s and impact angle is 15° (Autodyn).

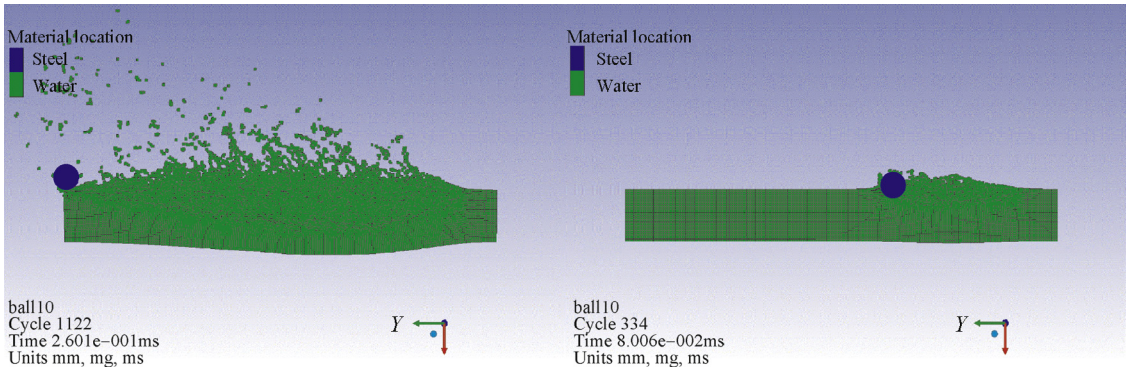

Fig. 8. Ricochet of a steel sphere of radius $a = 0.6$ cm in water. Impact velocity is 850 m/s and impact angle is 5° (Autodyn).

term with $\tau = 0.00219$ s and $v_c = 80.16$ m/s (which gives the C_d of 0.3) in Eq. (1) a good fit is achieved as shown by the analytical results in Fig. 10. However, the viscosity of gelatin is much larger than for water and thus the Reynolds number is much smaller for the same velocity. The Reynolds number is $Re = va\rho/\eta$, where η is the viscosity. In the range 10^3–3×10^5 the drag coefficient of a sphere in a fluid is known to be 0.47. The drag coefficient of a sphere is 0.2 when the Reynolds number is larger than 3×10^5. We set that $v = 850$ m/s, $a = 0.25$ cm, $\rho = 1.0$ g/cm^3, and $\eta = 10^{-3}$ Pa s for water. This gives $Re = 2 \times 10^7$ in water, and a constant drag coefficient of 0.2 is to be expected. However, the viscosity of gelatin may be more like honey or ketchup say 0.1–10 Pa s as our suggestion (https://en.wikipedia.org/wiki/Viscosity). We use that the drag coefficient is dependent of the Reynolds number [53] and set that $C_d = C_d(Re) = C_d(va\rho/\eta)$. Next we solve Eq. (1) numerically with $\tau =$ infinite. The viscosity η is chosen to match the measurements. We find that $\eta = 0.5$ Pa s gives a good fit to the experiments as seen by the numerical solution in Figs. 10. Fig. 11 shows the velocity vs time. We see that the camera recordings span the velocity range of 50–884 m/s.

Fig. 12 shows the effective drag coefficient in gelatin. The Autodyn simulates too large drag coefficient both for the SPH and an Eulerian grid in the target when applying a water model as a substitute. This may suggest that even for gelatin, that shows much lower Reynolds number than water, a turbulence

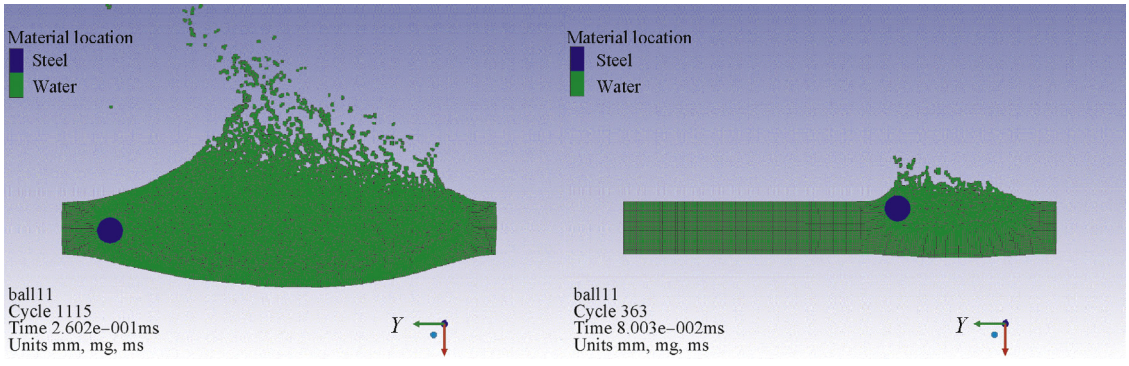

Fig. 9. Penetration of a steel sphere of radius $a = 0.6$ cm in water. Impact velocity is 850 m/s and impact angle is 10°.

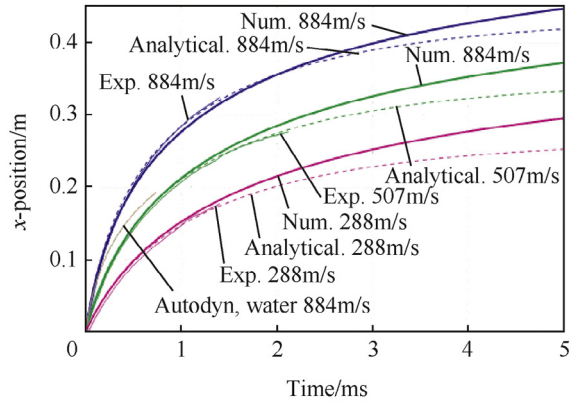

Fig. 10. Position vs time for a steel sphere of radius $a = 0.25$ cm penetrating into gelatin at different impact velocities. Exp shows high speed camera measurements. Num. is the numerical solution with the drag coefficient varying with the Reynolds number.

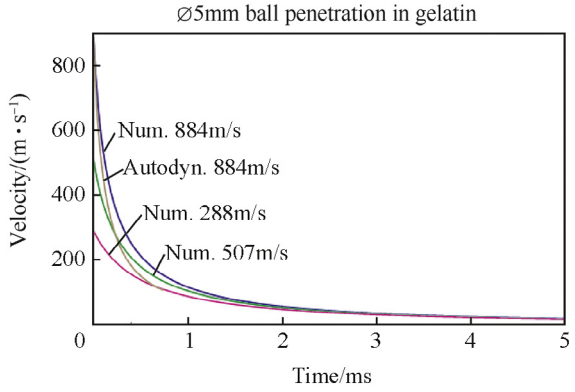

Fig. 11. Velocity vs time for a steel sphere of radius $a = 0.25$ cm penetrating into gelatin at different impact velocities. Num. is numerical solution with drag coefficient varying with the Reynolds number.

model is needed to reduce drag. Adding strain or strain rate dependency to the constitutive equation will increase the drag coefficients even more. We believe. However, the model and solver to be used in Autodyn to simulate the correct drag in water and in ballistic gelatin is uncertain.

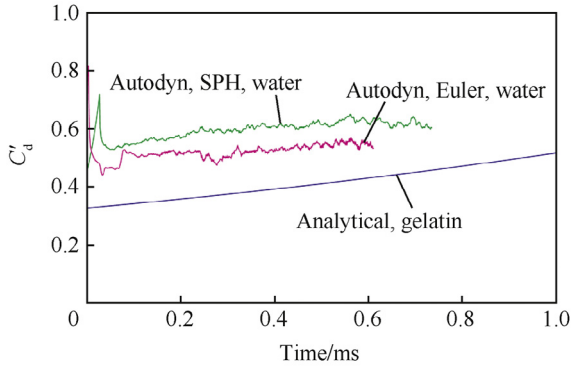

Fig. 12. The effective drag coefficient for a steel sphere of radius $a = 0.25$ cm penetrating into gelatin. The impact velocity is 884 m/s.

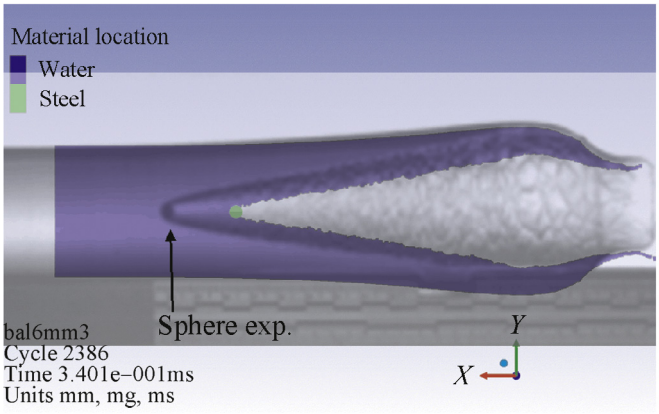

Fig. 13. Simulated and experimental results of a sphere with radius $a = 0.25$ cm penetrating into gelatin. The impact velocity is 884 m/s. The measured sphere (blue) is ahead of the simulated sphere in Autodyn SPH (green) with 2.7 cm. Using the Eulerian grid for gelatin the measured sphere is ahead of the simulated sphere with 1.7 cm.

Fig. 13shows the experimental results for the sphere and the cavity in gelatin. The experimental sphere is 2.7 cm ahead of the simulated sphere when using SPH and the water model as a model for gelatin. When using the Eulerian grid for gelatin the

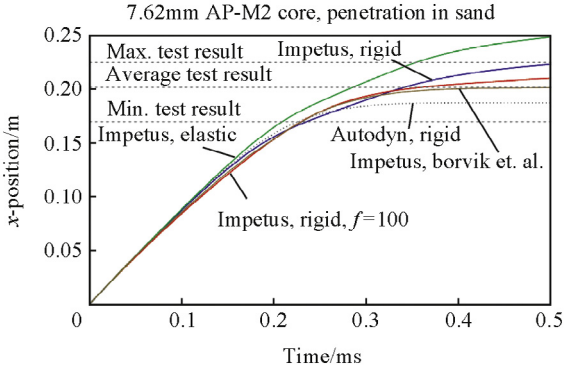

Fig. 14. The x-position vs time of a 7.62 mm APM2 core penetrating into sand. Impact velocity is 917 m/s.

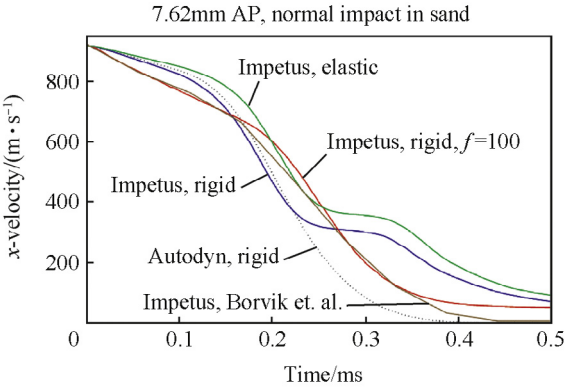

Fig. 15. The x-velocity vs time of a 7.62 mm APM2 core penetrating into sand. Impact velocity is 917 m/s.

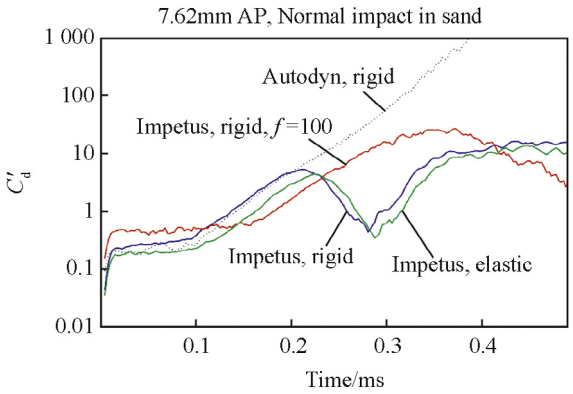

Fig. 16. The effective drag coefficient in x-direction for a 7.62 mm APM2 core penetrating into sand. Impact velocity is 917 m/s.

position of the simulated sphere is 1.7 cm behind the experimental position of the sphere.

2.4. 7.62 mm APM2

7.62 mm APM2 projectiles have been fired into sand by Børvik et al. [51]. The density of the sand was 1.73 g/cm^3. In the Autodyn simulation the sand bed is cylindrical with diameter 15 cm and length 30 cm. SPH particle size is 1.82 mm. We only model the hard core and not the jacket of the projectile as in Børvik et al. [51]. Fig. 14 shows the different simulation results together with the experimental results [51]. The Autodyn simulation fits very well. The reason may be that the resistance force due to the quadratic velocity dominates over the linear velocity resistance force due to the tumbling of the projectile. Thus effect of the linear resistance term may be much less significant than for the sphere. The elastic simulation in Impetus Afea Solver gives too large penetration distance. The rigid model fits better but still the penetration distance is too large. If we increase the penetration factor in the code by a factor of 100 (a numerical factor f related to resistance forces between boundaries) the penetration distance is closer to the results by Børvik et al. [51].

Fig. 15 shows the velocity vs time, while Fig. 16 shows the effective drag coefficient.

We use the axial x-velocity to estimate the drag coefficient. It is observed that due to tumbling the effective drag coefficient increases dramatically. Before the tumbling, the drag coefficient is around 0.5 or lower. It is notable that the rate of tumbling differs between the solvers.

Figs. 17 and 18 show the APM2 core penetration into sand simulated by Autodyn and Impetus Afea Solver respectively. We observe that only in Impetus Afea Solver does the projectile tumble 360°.

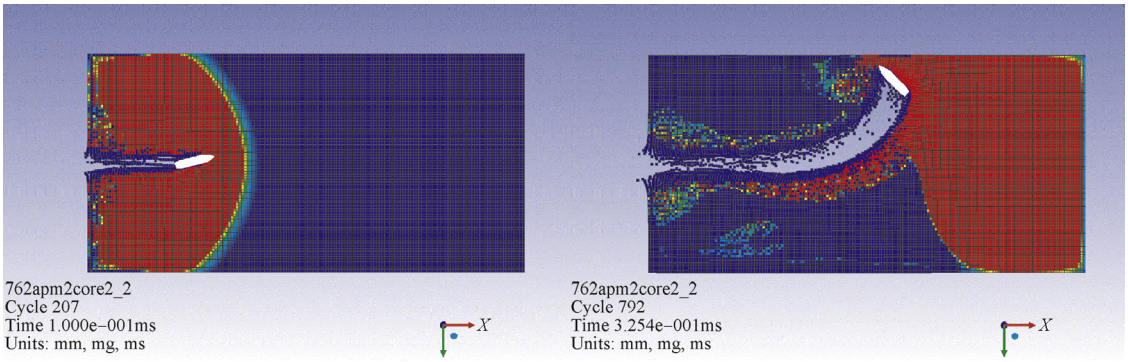

Fig. 17. 7.62 mm APM2 core penetrating into sand. Impact velocity is 917 m/s (Autodyn). Times are 0.1 ms and 0.325 ms.

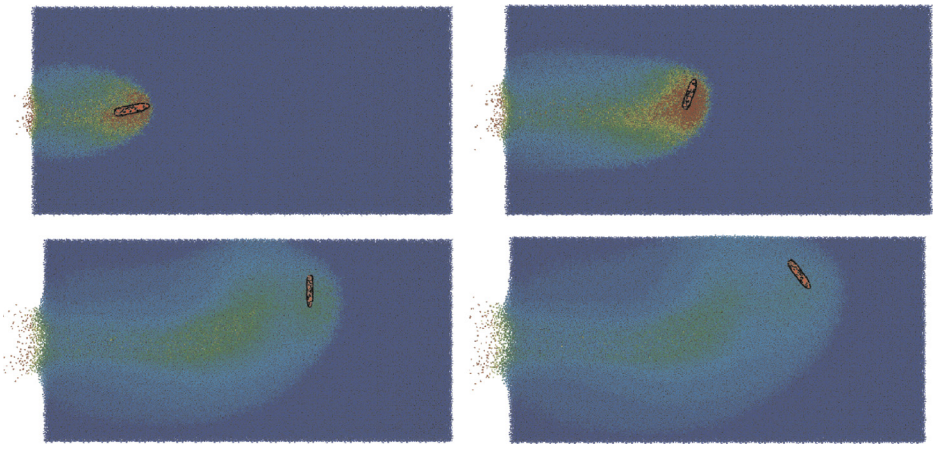

Fig. 18. 7.62 mm APM2 core penetrating into sand. Impact velocity is 917 m/s (Impetus Afea Solver). Times are 0.1 ms, 0.18 ms, 0.38 ms, and 0.48 ms.

2.5. 25 mm APEX projectiles

A 25 mm projectile is shot into sand at the impact velocity of 589 m/s, and the impact angles are 25° and 12.5°. The density of the sand is 1.67 g/cm^3. In the Autodyn simulation the sand bed size is 50 cm long, 15 cm deep and 4.5 cm wide (half symmetry). The SPH particle size is 1.5 mm. Fig. 19 shows the Autodyn simulation and Fig. 20 shows high speed camera pictures. Examination after recovery shows that the projectile is slightly deformed in the nose tip and this is not accounted for by the rigid model that we use. The experimental exit velocity of the sand is 111 m/s, while the simulated exit velocity is 154 m/s. The depth of the cavity was measured to be around 10 cm, which agrees with the maximum depth of the projectile simulated to be 12 cm. According to the camera recordings the projectile is into the sand during a length (measured along the sand bed) of 44 cm, which agrees well with the Autodyn simulation of 41 cm. By comparing Figs. 19 and 20 we see that the projectile in the Autodyn simulation exits the sand bed too early since the exit time should have been 3.7 ms and not 1.84 ms as simulated. Fig. 21 shows the Impetus Afea solver solution which shows results much equal to Autodyn. 5 million particles are used in the Impetus Afea Solver. The length of the bed is 60 cm. The depth is 20 cm, and the width is 5 cm. Fig. 22 shows the results for the impact angle of 12.5°. The simulated results are shown in Fig. 23. The measured exit velocity is 440 m/s while the simulated exit velocity is 408 m/s. Figs. 22 and 23 show good agreement for all times.

The CPU time is around 24 hours for the Autodyn simulation, but the Impetus Afea Solver simulation only use 1 hour due to the use of the graphic card on the computer. A very important reduction that means that ricochet simulations with elastic plastic deformation of the projectile is feasible.

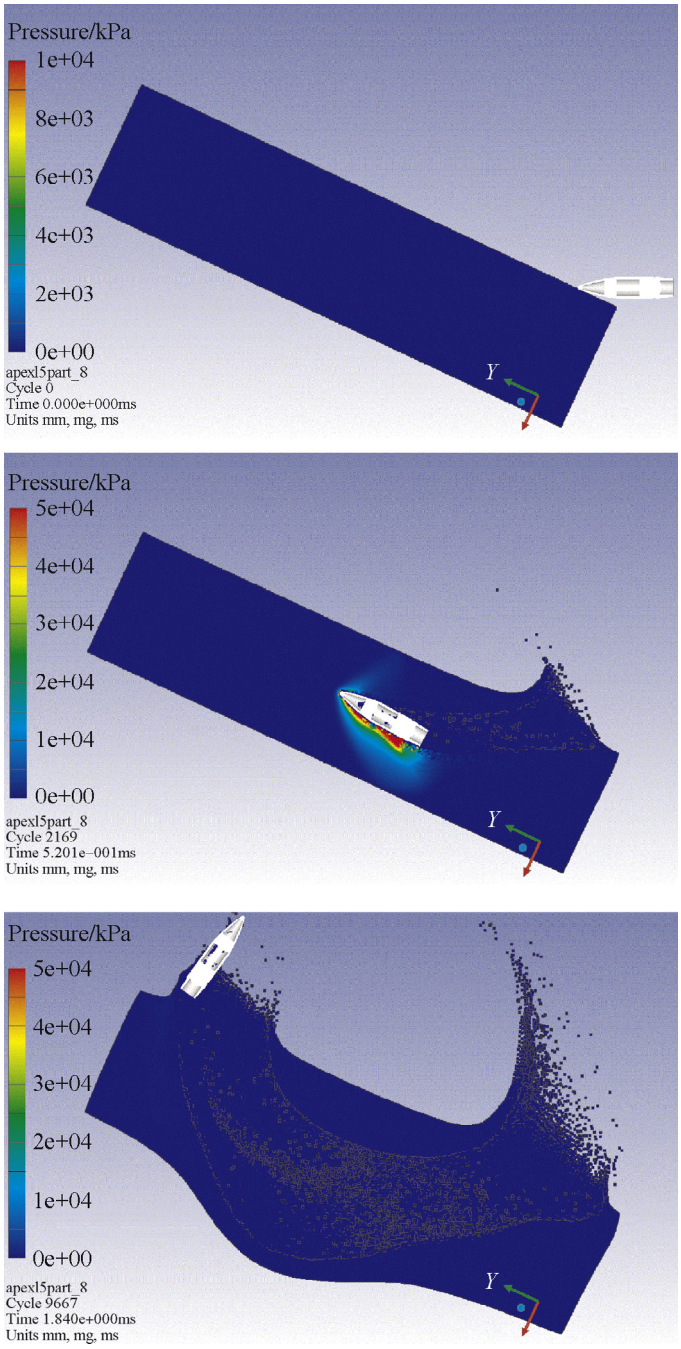

Fig. 19. Autodyn simulation of 25 mm projectile ricochet in sand. The impact velocity is 589 m/s and impact angle is 25° (Autodyn). The times are 0.0 ms, 0.52 ms, and 1.84 ms.

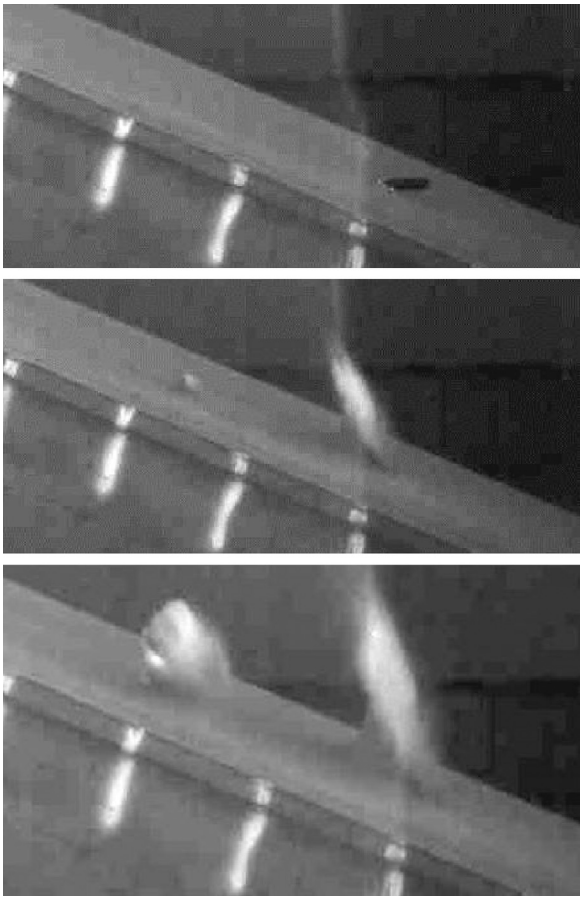

Fig. 20. Experiment of 25 mm projectile ricochet in sand. Impact velocity is 589 m/s and impact angle is 25°. The times are 0.0 ms, 1.84 ms, and 3.7 ms.

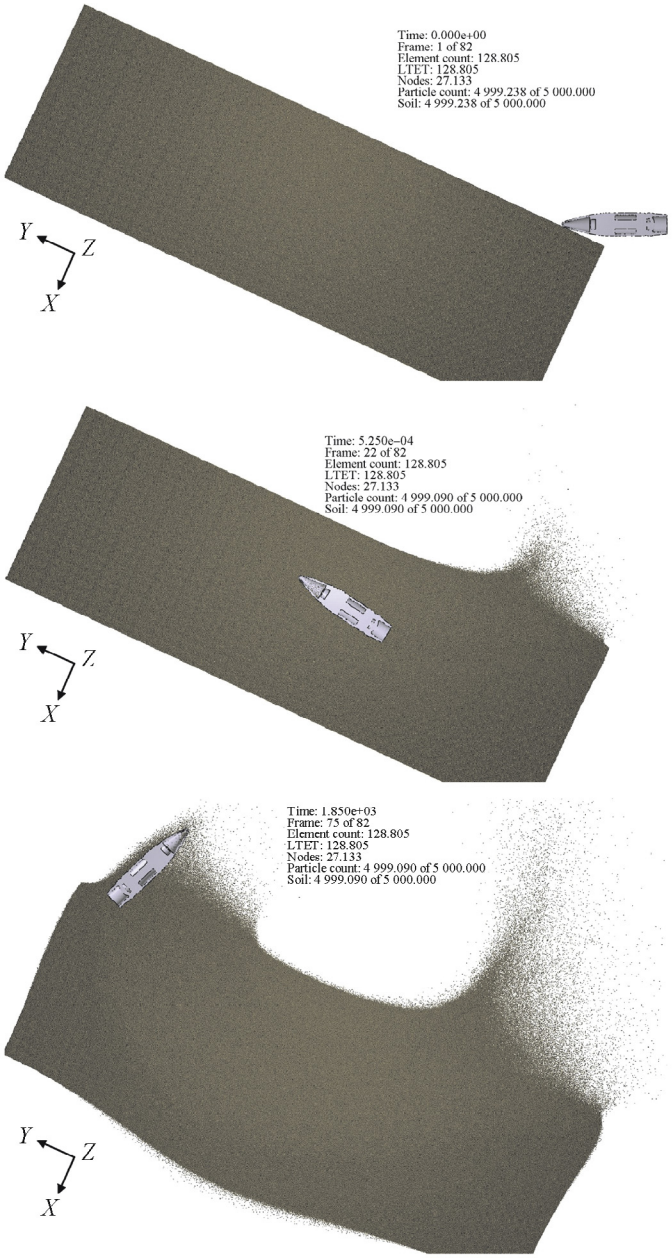

Fig. 21. Impetus Afea Solver simulation of 25 mm ricochet in sand. The impact velocity is 589 m/s and impact angle is 25°. The times are 0.0 ms, 0.53 ms, and 1.85 ms.

Fig. 22. Experiment of 25 mm projectile ricochet in sand. Impact velocity is 589 m/s and impact angle is 12.5°. The times are 0.0 ms, 0.3 ms, and 1.0 ms.

3. Conclusions and discussion

We have examined the ricochet and penetration behavior in sand and gelatin by steel spheres, 7.62 APM2, and 25 mm projectiles. The Autodyn simulation code with the SPH method, and the Impetus Afea Solver simulation code with the corpuscular model are used and the results are compared with experimental and analytical results. The resistance force in sand for spheres was found to proportional to a quadratic term in velocity plus a linear term in velocity. The drag coefficient for the quadratic resistance force was 0.65. The Autodyn and Impetus Afea Solver codes simulate too large penetration. We suggest that the reason is lack of a linear velocity resistance force. Critical ricochet angles were consistent with analytical results in the literature. In ballistic gelatin we study the penetration behavior in the velocity range of 100–850 m/s. A drag coefficient of 0.30 fits the high speed camera recordings if a linear velocity resistance term is added. However, only a quadratic velocity resistance force with drag coefficient that varies with the Reynolds number also fits to the measurements. The viscosity in gelatin is much higher than in water and a good estimate of the viscosity of gelatin is important due to the low Reynolds number numbers that gives Reynolds number dependency in the drag coefficient. The 7.62 mm APM2 core simulations in sand fit reasonable well for both codes. The tumbling rate essentially determines the penetration distance and linear velocity resistance forces seem less important. The simulation of a sphere in water with Autodyn and SPH showed too large drag coefficient. We believe that a turbulence model is needed to simulate the correct drag. The 25 mm projectile ricochet simulations show consistency with the high speed camera recordings although discrepancies were observed. Computer time was reduced by one to two orders of magnitudes when applying the Impetus Afea Solver compared to Autodyn code due to the use of the graphic card on the computer.

Our thorough literature survey, combined with the advanced numerical modeling using different types of solvers gives new

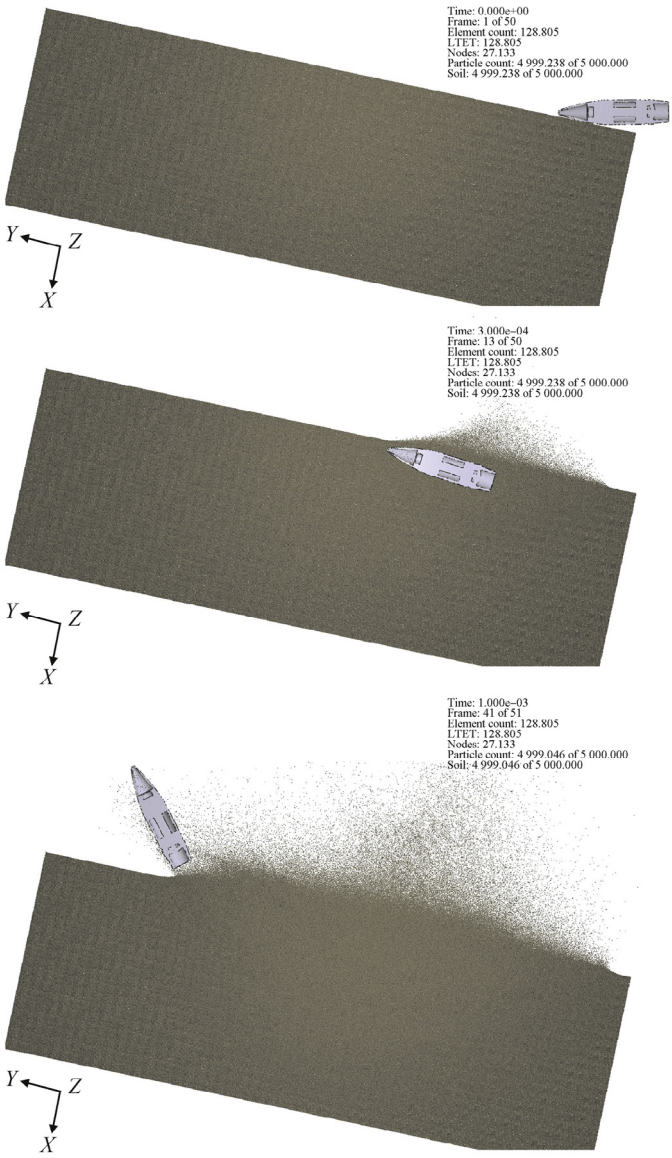

Fig. 23. Impetus Afea Solver simulation of 25 mm ricochet in sand. The impact velocity is 589 m/s and impact angle is 12.5°. The times are 0.0 ms, 0.3 ms, and 1.0 ms.

insight to the mechanisms and the quite complex problem of penetration and ricochet in multi-phase media such as sand as well as more homogeneous targets such as water and gelatin. Some confirming experiments were also made, and literature values were also used for comparison with the analytical and numerical results. It was interesting to see how the common Autodyn model performs relative to the more modern and higher order accurate Impetus Afea Solver one, and especially how the computational performance of the latter appears to be much more efficient on the computer.

We believe that the observed discrepancies between simulation results and experimental results are due to the mathematical models as such. The current continuum and corpuscular models in the literature for sand and gelatin needs more validation and probably also further development. The significant reduction in computer time when applying the Impetus Afea Solver, may in further studies, reveal the influence of projectile deformation and varying impact velocities during a lager range of impact angles. This brings the problem treated to a higher level.

Acknowledgment

The authors appreciate the comments from Chief Scientist Ove Dullum at Norwegian Defence Research Establishment, which have improved this paper.

Appendix A: MO granular model parameters

{Density [kg/m^3], Pressure [Pa]}:
{{1674, 0.0}, {1740, 4.58E+06}, {1874, 1.50E+07}, {1997, 2.92E+07}, {2144, 5.92E+07}, {2250, 9.81E+07}, {2380, 1.79E+08}, {2485, 2.89E+08}, {2585, 4.50E+08}, {2671, 6.51E+08}}
{Density [kg/m^3], Sound speed [m/s]}:
{{1674, 265.2}, {1746, 852.1}, {2086, 1721.7}, {2147, 1875.5}, {2300, 2264.8}, {2572, 2956.1}, {2598, 3112.2}, {2635, 4600.0}, {2641, 4634.0}, {2800, 4634.0}}
{Pressure [Pa], Yield stress [Pa]}:
{{0.0, 0.0}, {3.40E+06, 4.24E+06}, {3.49E+07, 4.47E+07}, {1.01E+08, 1.24E+08}, {1.85E+08, 2.26E+08}, {5.00E+08, 2.26E+08}}
{Density [kg/m^3], Shear modulus [Pa]}:
{{1674, 7.69E+07}, {1746, 8.69E+08}, {2086, 4.03E+09}, {2147, 4.91E+09}, {2300, 7.77E+09}, {2572, 1.48E+10}, {2598, 1.66E+10}, {2635, 3.67E+10}, {2641, 3.73E+10}, {2800, 3.73E+10}}

Appendix B: The Impetus Afea cap model

The base line and the cap model in Impetus Afea set the friction force between particles as

$$F_f = \mu_s F_N = \mu_s K_s \delta, \; Base\ line, \; K_s = 4\,10^8 \; N/m$$
$$F_f = \mu_s F_N = \mu_s K_s Min(\delta, 2R\eta_s), \; Cap \qquad \text{(B1)}$$

For the baseline model $\mu_s = 0.1$. For the cap model $\mu_s = 0.8$, $\eta_s = 0.008$. R is the particle size.

References

[1] Pierazzo E, Melosh HJ. Understanding oblique impacts from experiments, observations, and modeling. Annu Rev Earth Planet Sci 2000;28:141–7.
[2] Braslau DJ. J Geophys Res 1970;75:3987–99.
[3] Nakata Y, Hyodo M, Hyde AFL. Microscopic particle crushing of sand subjected to high pressure one-dimensional compression. Soils Found 2001;41:69–82.
[4] Parab ND, Claus B, Hudspeth MC, Black JT, Mondal A, Sun J, et al. experimental assessment of fracture of individual sand particles at different loading rates. Int J Impact Eng 2014;8:14.
[5] Omidvar M, Iskander M, Bless S. Response of granular media to rapid penetration. Int J Impact Eng 2014;66:60–82.
[6] Robins B. New principles of gunnery. Richmond, Surrey: Richmond Publishing Co. Ltd; 1972.
[7] Euler L. Neue grundsätze der artillerie. Berlin: Von B.G. Teubner; 1922.
[8] Poncelet JV. Cours de Mécanique Industrielle. 1829.
[9] Resal H. Sur la penetration d'un projectile dans les semifluids it les solides, cr. 120:397–401. 1895.

[10] Forrestal MJ, Luk VK. Penetration into soil targets. Int J Impact Eng 1992;12:427–44.
[11] Allen WA, Mayfield EB, Morrison HL. Dynamics of a projectile penetrating sand. J Appl Phys 1957;28(3):370–6.
[12] Soliman AS, Reid SR, Johnson W. The effect of spherical projectile speed in ricochet off water and sand. Int J Mech Sci 1976;18:279–84.
[13] Bernard RS, Creighton DC. Projectile penetration in soil and rock: analysis for non-normal impact. Vicksburg, MS, USA: U.S. Army Engineer Waterways Experimental Station Structures Laboratory; 1979. p. 12–60. Technical Report SL-79-15.
[14] Daneshi GH, Johnson W. The ricochet of spherical projectiles off sand. Int J Mech Sci 1977a;19:491–7.
[15] Daneshi GH, Johnson W. The ricochet of dumb-bell shaped projectiles. Int J Mech Sci 1977b;19:555–63.
[16] Bai YL, Johnson W. The effect of projectile speed and medium resistance in ricochet in sand. J Mech Eng Sci 1981;23:69–75.
[17] Johnson W, Sengupta AK, Ghosh SK. High velocity oblique impact and ricochet mainly of long rod projectiles: an overview. Int J Mech Sci 1982;24(7):425–36.
[18] Savvatteev AF, Budin AV, Kolikov VA, Rutberg PG. High-speed penetration into sand. Int J Impact Eng 2001;26:675–81.
[19] Anderson JLB, Schultz PH. Flow-field center migration during vertical and oblique impacts. Int J Impact Eng 2006;33:35–44.
[20] Dwivedi SK, Teeter RD, Felice CW, Gupta YM. Two dimensional mesoccale simulations of projectile instability during penetration in sand. J Appl Phys 2008;104:083502.
[21] Bless SJ, Berry DT, Pedersen B, Lawhorn W. Sand penetration by high speed projectiles. AIP Conf Proc 2009;1195:1361.
[22] Nishida M, Okumura M, Tanaka K. Effects of density ratio and diameter ratio on critical angles of projectiles impacting granular media. Granular Matter 2010;12:337–44.
[23] Li QM, Flores-Johnson EA. Hard projectile penetration and trajectory stability. Int J Impact Eng 2011;38:815–23.
[24] Ye X, Wang D, Zheng X. Influence of particle rotation on the oblique penetration in granular media. Phys Rev E 2012;86:061304.
[25] Collins AL, Addiss JW, Walley SM, Promratana K, Bobaru F, Proud WG, et al. The effect of rod nose shape on the internal flow fields during the ballistic penetration in sand. Int J Impact Eng 2011;38:951–63.
[26] Wen Y, Xu C, Wang H, Chen A, Batra RC. Impact of steel spheres on balletic gelatin at moderate velocities. Int J Impact Eng 2013;62:142–51.
[27] Moxnes JF, Ødegårdstuen G, Atwood A, Curran P. Mechanical properties of a porous material studied in a high speed piston driven compaction experiment. In: 30th ICT. Karlsruhe: Frauenhofer ICT; 1999.
[28] Grujicic M, Pandurangan B, Cheeseman B. The effect of degree of saturation of sand on detonation phenomena associated with shallow-buried and ground-laid mines. Shock Vib 2006;13:41–61.
[29] Omidvar M, Iskander M, Bless S. Stress-strain behavior of sand at high strain rates. Int J Impact Eng 2012;49:192–213.
[30] Laine L, Sandvik A. Derivation of mechanical properties for sand. In: Proceedings of the 4th Asia-Pacific conference on shock and impact loads on structures. Singapore: CI-Premier PTE LTD; 2001. p. 361–8.
[31] Grujicic M, Pandurangan B, Qiao R, Cheeseman BA, Roy WN, Skagg RR, et al. Parameterization of the porous-material model for sand with different levels of water saturation. Soil Dyn Earthq Eng 2008;28:20–35.
[32] Fairlie G, Bergeron D. Numerical simulations of mine blast loading on structures. In: 17th numerical aspects of blast symposium. Las Vegas, Nevada: 2002.
[33] Tjernberg A. Simulation of mine-blast deflection. Tumba, Sweden: FOI-Swedish Defence Research Agency; 2006. Technical Report, FOI-R-1913-SE.
[34] Wu W, Thomson R. A study of the interaction between a guardrail post and soil during quasi-static and dynamic loading. Int J Impact Eng 2007;34:883–98.
[35] Laine L, Larsen OP. Implementation of equation of state for dry sand in Autodyn. In: 83th proceedings of shock and vibration symposium, shock and vibration exchange. New Orleans, Louisiana: Shock and Vibration Exchange; 2012.
[36] Grujicic M, Bell WC, Marvi H, Haque I. A computational analysis of survivability of a pick-up truck subjected to mine detonation loads. Multidiscip Model Mater Struct 2011;7(4):386–423.
[37] Wang Z, Hao H, Lu Y. A three phase soil model for simulating stress wave propagation due to blast loading. Int J Numer Anal Methods Geomech 2004;28:33–56.
[38] Zakrisson B, Haggblad H-A, Jonsen P. Modelling and simulation of explosions in soil interacting with deformable structures. Cent Eur J Eng 2012;2(4):532–50.
[39] Tong X, Tuan C. Viscoplastic cap model for soils under high strain rate loading. J Geotech Geoenviron Eng 2007;133(2):206–2014.
[40] Higgins W, Chakraborthy T, Basu D. A high strain-rate constitutive model for sand and its application in finite-element analysis of tunnels subjected to blast. Int J Numer Anal Methods Geomech 2013;37:2590–610.
[41] Andò E, Hall SH, Viggiani G, Desrues J, Besuelle P. Grain-scale experimental investigation of localized deformation in sand: a discrete particle tracking approach. Acta Geotech 2012;7:1–13.
[42] Borg JP, Vogler TJ. Rapid compaction of granular material: characterizing two-and three-dimensional mesoscale simulations. Shock Waves 2013;23:153–76.
[43] Lammi CJ, Vogler TJ. Mesoscale simulations of granular materials with peridynamics. AIP Conf Proc 2011;1426:1467. doi:10.1063/1.3686599.
[44] Deshpande VS, McMeeking RM, Wadley HNG, Evans AG. Constitutive model for prediction dynamic interactions between soil ejecta and structural panels. J Mech Phys Solids 2009;57:1139–64.
[45] Bagnold RA. Experiments on a gravity-free dispersion of large solid particles in a Newtonian fluid shear. Proc R Soc Lond A Math Phys Sci 1954;225:49–63.
[46] Børvik T, Olovsson L, Hansen AG, Dharmasena KP, Hansson H, Wadley HNG. A discrete particle approach to simulate the combined effect of blast and sand impact loading of steel plates. J Mech Phys Solids 2011;59:940–58.
[47] Olovsson L. Corpuscular method for airbag deployment simulations in LS-Dyna. Huddinge: Impetus Afea AB; 2007. ISBN 978-82-997587-0-3.
[48] Olovsson L, Hanssen AG, Børvik T, Langseth M. A particle-based approach to close-range blast loading. Eur J Mech A Solids 2010;29:1–6.
[49] Anderson CE, Behner T, Weiss CE. Mine blast loading experiments. Int J Impact Eng 2011;38:697–706.
[50] Johnson GR, Beissel SR, Gerlach CA. Another approach to a hybrid particle-finite element algorithm for high-velocity impact. Int J Impact Eng 2011;38(397):405.
[51] Børvik T, Dey S, Olovsson L. Penetration of granular materials by small-arms bullets. Int J Impact Eng 2015;75:123–39.
[52] Saslow WM, Lu H. Newton on objects moving in a fluid-the penetration length. Eur J Phys 2009;29:689–96. doi:10.1088/0143-0807/29/4/004.
[53] Landau LD, Lifshitz EM. Fluid mechanics, course of theoretical physics, vol. 6. England: Pergamon Press; 1982. p. 171.